Hypervelocity Impact Testing of IM7/977-3 with Micron-Sized Particles

J.G. Smith Jr.*, D.C. Jegley†, and E.J. Siochi‡
NASA Langley Research Center, Hampton, VA 23681-2199

B. K. Wells§
Auburn University, Auburn, AL 36849

Ground-based hypervelocity impact testing was conducted on IM7/977-3 quasi-isotropic flat panels at normal incidence using micron-sized particles (i.e. ≤ 100 μm) of soda lime glass and olivine. Testing was performed at room temperature (RT) and 175°C with results from the 175°C test compared to those obtained at RT. Between 10 and 30 particles with velocities ranging from 5 to 13 km/s impacted each panel surface for each test temperature. Panels were ultrasonically scanned prior to and after impact testing to assess internal damage. Post-impact analysis included microscopic examination of the surface, determination of particle speed and location, and photomicroscopy for microcrack assessment. Internal damage was observed by ultrasonic inspection on panels impacted at 175°C, whereas damage for the RT impacted panels was confined to surface divets/craters as determined by microscopic analysis.

I. Introduction

On January 14, 2004, President Bush put forth a new U.S space policy entitled "Vision for U.S. Space Exploration" and charged NASA with its implementation. One part of that vision described an eventual return and sustained presence on the Moon. To accomplish this task a new suite of vehicles similar in design to the Apollo-era crafts, but much larger in size, were proposed. Due to vehicle size and mass allowances, an overall need for increased usage of light-weight materials [e.g. Fiber Reinforced Polymeric Composites (FRPCs)] are required in their construction. Over the past few decades FRPCs have been increasingly used on space vehicles due to their low weight as well as their high stiffness and specific strength.[1-3] Their low weight provides a mass savings that is crucial for space vehicles, where launch costs can be as high as tens of thousands of dollars per pound. Current vehicle applications include optical benches, antenna struts, structural panels, and low distortion frames on unmanned vehicles and satellites, robotic arm and cargo doors of the Space Shuttle, and the Space Station Remote Manipulator System.[2,3]

Due to time constraints in the program, material selection was limited to those that were Commercial-Off-The-Shelf (COTS) for evaluation. A limited number of these COTS materials were space-qualified with the vast majority being only aircraft-qualified. It was anticipated that the COTS materials that were only aircraft-qualified could be deemed usable for several anticipated space applications with the determination of additional properties obtained under relevant conditions. One property of interest is the susceptibility of FRPCs to impact damage caused by materials traveling at hypervelocity.

Damage sustained by spacecraft from objects traveling at hypervelocity, both natural and man-made, has been of interest since the advent of the space age. Naturally occurring debris consists of particles from comets, asteroids, and other cosmic dust particles of various sizes and elemental compositions.[4] The majority of this natural debris range in size from 1 to 500 μm[5]. Man-made debris includes by-products of normal spacecraft operation, fragments from vehicle collisions, paint, etc.[6] and can range in size from microns to meters. It has been reported that the low Earth orbit (LEO) velocity of this debris is on the order of 7-11 km/s.[4] Debris that is micron size and smaller have been found to degrade mirrored surfaces on sensors while those that are tens to hundreds of microns in size can penetrate solar cells, outer coatings, and foils.[5] Particles of this size are quite abundant in low Earth orbit and are

* Sr. Polymer Scientist, Advanced Materials and Processing Branch, MS 226
† Sr. Aerospace Engineer, Structural Mechanics and Concepts Branch, MS 190, AIAA Associate Fellow
‡ Supervisory Aerospace Engineer, Advanced Materials and Processing Branch, MS 226
§ Research Associate, Space Research Institute, 231 Leach Science Center

virtually undetectable.[5] For example, damage from particles 8 to 80 μm in size has been observed as impact craters whose 'conchoidal cracking' or 'spall' diameters range from 100 to 1000 μm on solar cells of solar panels returned from the Hubble Space Telescope (HST).[6] Of greatest concern are particles that are one cm or larger in size and traveling at hypervelocity which can penetrate a vehicle's structure, potentially leading to catastrophic failure.

In order to understand the effects of hypervelocity impact (HVI) by materials on vehicle surfaces with the objective of improving structural durability, ground-based studies have been conducted. Early research focused on metals, ceramics, and glasses, while more recent research has been conducted on aerospace quality FRPCs. The work reported herein concerns HVIs on a COTS FRPC. A brief review of HVI research as it relates to FRPCs is provided below. For a more comprehensive treatise, it is suggested that the reader turn to the vast body of literature available on the subject.

HVI damage is dependent upon impactor size and velocity as well as the construction of the vehicle (e.g. material, thickness, sensitivity to failure).[4,5] In general, the HVI episode lasts a few microseconds, creating a shock wave that can afford pressures >100 GPa and temperatures >10,000 K, both of which are highly dependent upon the impact velocity.[5] Craters formed from these impacts are generally hemispherical in shape and often two to five times greater in size than the impactor in ductile materials (i.e. metals) and ten to twenty times greater in size in brittle materials. Damage caused by an HVI event does not need to fully penetrate the vehicular structure to be of concern. For example, the creation of breaks in surface coatings may permit atomic oxygen erosion in low Earth orbit (LEO). Regarding FRPCs, damage can include delamination, surface/rear spallation and laminate penetration.[1] In addition, relatively minor levels of damage (often referred to as Barely Visible Impact Damage) can cause leak paths to develop leading to the internal structure's exposure to the space environment.

Ground based HVI studies of FRPCs evaluated to date have focused on epoxy and polyether ether ketone matrices with various fibers [e.g. carbon (AS-4, IM6), Spectra 900, and Kevlar].[1,3,7-11] Test article configurations have been predominantly flat plate, tubes/cylinders, and composite laminate/sandwich structure with much of the work conducted on flat plate. A majority of these tests used impactors in the cm size resulting in catastrophic damage. However, a report is available on the effect of micron-sized impactors.[7]

To validate ground-based studies, space exposure tests are conducted when feasible. One such space exposure test of FRPCs was on the Long Duration Exposure Facility (LDEF) where epoxy-based materials were exposed to the LEO environment for 5.75 years prior to retrieval. With respect to HVIs, the FRPCs incurred 74 impacts from orbital debris with craters <0.5 mm (i.e. 500 μm) in size and 10 impacts ≥0.5 mm in size.[12,13] One observation noted from these impacted samples was that the debris could penetrate 4-ply laminates with substantial rear face spallation.[12] These results as well as subsequent ground-based studies conducted by the University of Toronto Institute for Aerospace Studies have been compiled into an extensive database with the aim of creating comprehensive damage models for characterization of HVI micrometeoroid/orbital debris damage.[2,3]

Due to the difficulty in performing HVI tests, most of the research has been conducted at room temperature (RT). However, the actual space environment is not limited to this temperature. Satellite surface temperatures can range from ±150°C,[14] while Lunar surface temperatures can range from a low of -173°C during the night to a high of 127°C during the day.[15] Recent work has examined differences in HVI damage between RT and elevated (i.e. 110 and 210°C) temperatures.[16] It was found that hole diameters were larger for heated materials compared to RT. This temperature dependence was most prominent for impact speeds of 2-4 km/s and decreased with increasing impact velocity. Results from low temperature testing were comparable to RT results with regard to hole size but the shape and structure of the impact was more complex.[17,18]

On the Moon, micrometeoroid impacts have been calculated to have a strong mass flux at ~ 1.5×10^{-5} g corresponding to a particle diameter of approximately 220 μm with an average derived velocity of 13.3 km/s.[19] HVI damage can also occur from Lunar regolith jettisoned from the surface by large meteor impacts and vehicular landings. Lunar regolith consists primarily of olivine, pyroxene, and plagioclase feldspar with a mean grain size between 45 and 100 μm.[20,21] Recent re-evaluation of film footage from the Apollo Lunar Module landings suggested that some of the "kicked-up" regolith could be accelerated to velocities as high as 1.5 km/s. This "regolith kick-up" event was evident on hardware returned from Surveyor 3 by Apollo 12 where microcraters were found to be generated from particles as large as 60 μm.[22]

Since it is anticipated that there will be significant usage of FRPCs on the Lunar surface due to vehicle mass considerations and based on the damage observed on LDEF, HST and Surveyor 3, a study was initiated to examine HVI effects on a FRPC at RT and 175°C using micron-sized particles (i.e. soda lime glass and olivine). In the construction of the Orion command module, IM7/977-2 was selected. IM7/977-2 has a dry operational temperature of 138°C which is lower than the space upper thermal extreme.[23] This FRPC would be covered by a thermal protection system on Orion so IM7/977-2 is an acceptable choice. For unprotected FRPCs a higher use temperature

material is needed. Therefore, IM7/977-3 with a dry use temperature of 177°C was selected for this study.[24] This is a toughened epoxy system used in aircraft primary/secondary structures where impact resistance is needed. HVI temperature effects were evaluated using two types of micron-sized impactors that were impacted on quasi-isotropic panels of IM7/977-3 with the results reported herein.

II. Experimental

A. Test Specimens[⌘]

Two 24-ply quasi-isotropic $[\pm 45/0/90]_{ns}$ panels 25.4 cm x 66.04 cm and approximately 0.635 cm thick were fabricated from Cytec Engineered Materials HYE IM7/977-3 prepreg using the standard cure cycle recommended by the manufacturer. Test articles (20.32 cm x 20.32 cm) were subsequently machined from each panel (Fig. 1). In each corner of the test article, a 0.635 cm diameter mounting-hole was drilled 1.27 cm from the panel end. The panels were then ultrasonically scanned (C-scan) prior to shipment for HVI testing. Material properties reported in Refs. 24 and 25 for IM7/977-3 are shown in Table 1. The 977-3 system has a reported minimum T_g as determined by DMA (5°C/min, G′) of 190°C resulting in a dry service temperature of 177°C.[24] The change in material properties with temperature indicates that there may be differences in the material's response to impact damage depending on the thermal environment at the time of impact.

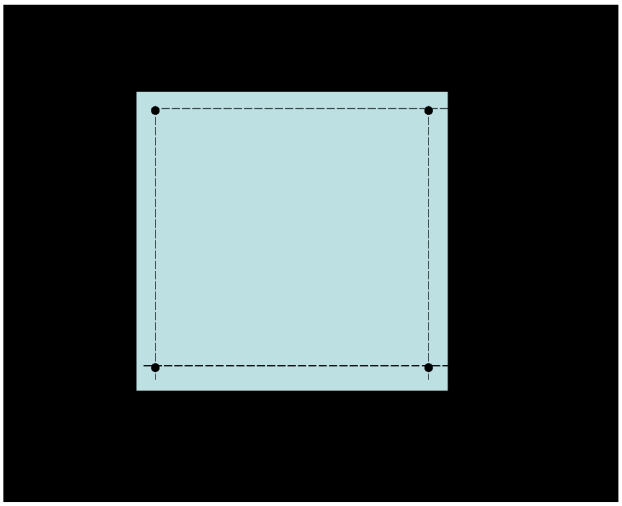

Figure 1. IM7/977-3 test panel configuration.

Table 1. Composite Properties [Ref. 24].

Property	Test Temperature, °C						
	-60	25	104	121	132	149	165 [Ref. 25]
0° Tensile Str., MPa	2430	2510 3578[25]	-----	-----	-----	-----	3144
0° Tensile Mod., GPa	158	162 188[25]	-----	-----	-----	-----	208
90° Tensile Str., MPa	-----	64.1 55.8[25]	-----	-----	-----	-----	37.2
90° Tensile Mod., GPa	-----	8.34 11.0[25]	-----	-----	-----	-----	5.5
0° Compressive Str., MPa	-----	1680	-----	-----	-----	-----	-----
0° Compressive Mod., GPa	-----	154	147	141	139	148	-----
0° Flex Str., MPa	-----	1765	1700	1524	1500	1420	-----
0° Flex Mod., GPa	-----	150	153	143	145	145	-----
Inter Laminar Shear Str., MPa	-----	128	94	92	85	79	-----

Each pre- and post-impact test article was subjected to ultrasonic inspection using a 3 axis (x, y and z) Ultrasonic Scanner from SONIX Advanced Acoustic Solutions using WIN IC (C-Scan) Version 4.1.0k software. A Panametrics transducer of 15 MHz/0.635 cm diameter and 3.175 cm focal length was used. A conventional

⌘ The use of trade names or manufacturers does not constitute an official endorsement of such products or manufacturers, either expressed or implied, by the National Aeronautics and Space Administration.

ultrasonic pulse-echo C-scan method was used for detecting delaminations with the gain set to 41 dB. C-scan images indicated that all panels were well consolidated prior to impact testing.

B. Impactors

Two types of impactors were used in this study: Soda Lime Glass (SLG) to represent man-made debris and OLiVine (OLV) to represent the natural environment. OLV is a constituent of stony meteorites[26] as well as Lunar regolith.[20,21] In Lunar regolith the particle size ranges from sub-micron up to large rocks, with the majority being micron-sized.

SLG particles are readily available from the metal polishing industry and exhibit minimal fracturing during HVI testing allowing for accurate size determination of the impactor during post-impact analysis. Prior to loading in the gun the SLG particles were sieved from a bulk lot into multiple bins. Samples from each bin were mixed on an equal volume basis and placed on the gun breach support film. Images were then obtained under magnification to determine particle diameters so as to verify that a reasonable distribution of each volume fraction was loaded in the gun. A representative image of the particles on the support film is shown in Fig. 2. In general, the particles were spherical with an average diameter of 68 μm (Table 2).

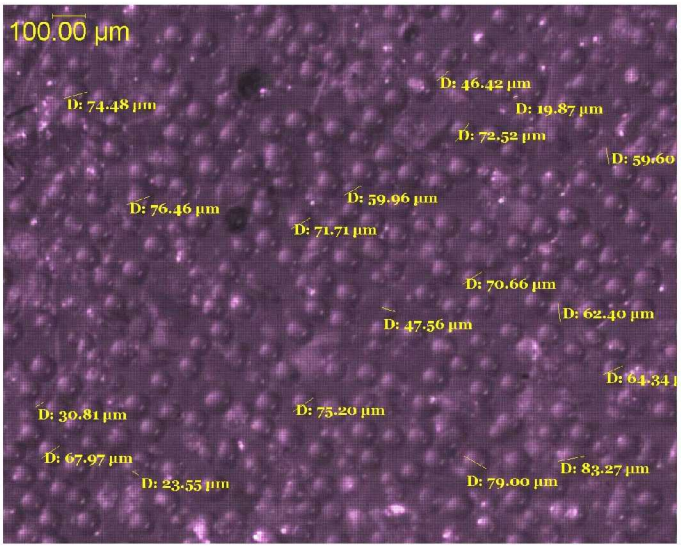

Figure 2. SLG Particles under magnification.

Table 2. SLG Particle Diameter.

Particle #	Diameter, μm
1	33.08
2	33.63
3	46.84
4	50.67
5	54.61
6	56.92
7	59.85
8	61.50
9	66.03
10	68.97
11	69.01
12	70.81
13	72.84
14	75.10
15	76.79
16	77.95
17	82.47
18	82.60
19	83.74
20	83.80
21	86.92
22	87.33
23	92.19
Average	68.42
Minimum	33.08
Maximum	92.19

Whereas SLG is spherical, OLV is irregularly shaped. It is also denser than SLG (i.e. density of 3.2 vs. 2.4 g/cm^3, respectively) and as a consequence may be accelerated at lower velocities during testing. In addition the particles have the potential to fracture prior to impact on the sample surface, making post-impact analysis challenging.[26] The OLV particles were selected from several lots of screened material to afford particles with diameters predominantly <150 μm in size (Table 3). A representative image of the particles on the support film is shown in Fig. 3.

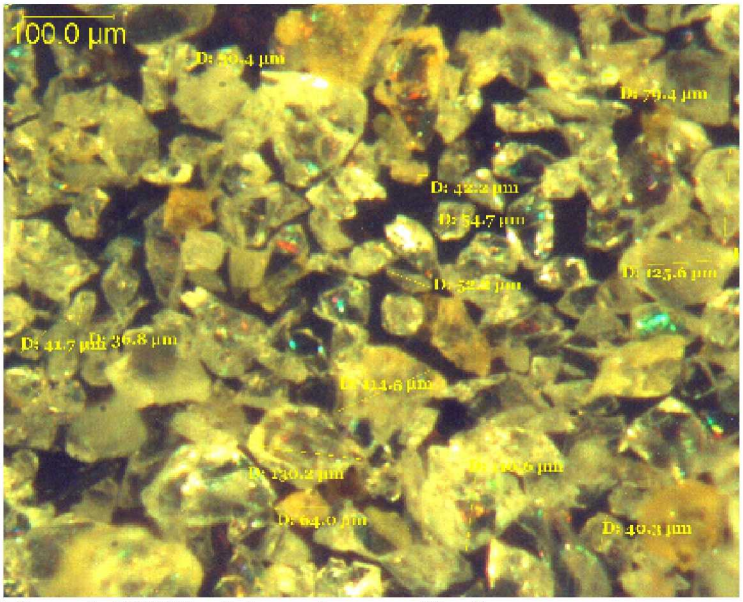

Figure 3. OLV Particles under magnification.

Table 3. OLV Particle Diameter.

	RT	175°C
Particle #	Diameter, µm	
1	43.1	30.4
2	44.1	36.8
3	52.8	40.3
4	53.1	41.7
5	60.6	42.2
6	61.8	52.2
7	66.3	54.7
8	70.9	64
9	72.2	79.4
10	77.9	99.7
11	96.6	110.6
12	118	114.5
13	121.2	125.6
14	122.1	130.2
15	140.1	
16	169.4	
Average	83.8	73.0
Minimum	43.1	30.4
Maximum	169.4	130.2

C. Hypervelocity Impact (HVI) Testing

Four test articles were subjected to HVI testing at the Hypervelocity Impact Facility located at Auburn University's Space Research Institute under NASA contract NNL07AJ01P. HVI testing was performed at RT and 175°C. Details of the experimental set-up can be found in Ref. 26, but are briefly described here. The target chamber dimensions are 1.22 m in diameter by 1.22 m long. The impact area is a 15 cm diameter circle centered on the bore of the gun flight tube. An anodized plate installed in the target chamber is used to mount samples for room and elevated temperature tests. All impacts are conducted under vacuum (10^{-6} Torr) utilizing a plasma drag gun. On average, the gun delivers 5 to 50 particles to the target surface per test at normal incidence at velocities ranging from 5 to 12 km/s. High-speed images are captured using a streak camera and photomultiplier tube detection system during the test, which allows for the speed, based on the target distance, and location of each impacting particle to be identified. Additionally, a 0.6 µm thick Mylar® ballistic witness film placed in front of the sample is used to determine the impactor diameter just prior to striking the sample.

The FRPC was mounted in the target chamber using three of the four mounting holes. Four LED's were secured across the top and left side edge of the sample to provide reference points on the data acquisition images with the location of each marked with a marking pen. For the soda lime glass test conducted at 175°C (SLG ET), the FRPC was heated with two 2500 W infrared heat lamps pointed at the front and the back of the sample. The diameter of the heat lamp was 12.7 cm. Temperature measurements were made using Lakeshore silicon diode sensors. For the olivine test conducted at 175°C (OLV ET), the panel was heated with a heat tape mounted on the back of the FPRC and an IR lamp on the front.

Once the gun is fired, particles are accelerated along numerous trajectories with only a very small fraction of the loaded particles traveling toward the target. This process randomly selects a few particles of varying size to reach the target. As a consequence, the particles impacting the surface are not generally representative of the initial range or distribution shown in Tables 2 and 3.

D. Post-Impact Analysis

Post-test evaluation included ultrasonic, visual and microscopic evaluation of the surface, and photomicrography of sectioned FRPCs. Internal delamination caused by the reflection of stress waves from the inter-ply interfaces inside the FRPCs due to HVI has been shown to be detectable by ultrasonic inspection (i.e. C-scan).[3] The impactor/particle size and impact energies were calculated based on test data. Examination of the witness film after the test allowed for determination of particle impact locations on the panel. The impact locations, in mm, were referenced to the bottom left corner of the composite test panel. The particle dimension associated with the

identified impact location was obtained from measurement of the residual "hole" in the witness film as shown in Fig. 4. The measurements a and b refer to the diameter in μm of the longest and shortest axes of the witness film hole.

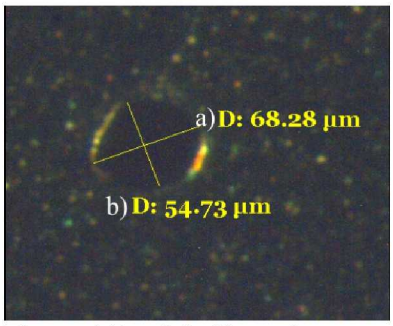

Figure 4. Particle dimensions.

These dimensions were subsequently used to calculate the particle area in μm^2 based on a sphere using Eq. 1:

$$\text{Particle area} = 4\pi(a/2)(b/2) \quad (1)$$

This method is highly accurate for spherical particles. However, the non-uniform aspect ratio for irregularly shaped particles such as OLV can result in uncertainty in the diameters, volume and consequently mass and energy of the particle upon impact.

The particle diameter in μm and mass in kg were then calculated using Eqs. 2 and 3, respectively:

$$\text{Particle diameter} = 2(\text{particle area}/\pi)^{0.5} \quad (2)$$

$$\text{Particle mass} = (\rho_{particle})(4/3)\pi(\text{particle radius})^3 \quad (3)$$

where the radius was in cm and the particle density (ρ) was 0.0024 kg/cm^3 for SLG and 0.0032 kg/cm^3 for OLV. The energy in Joules was then calculated using the derived particle mass and associated velocity using Eq. 4:

$$E = 0.5mv^2 \quad (4)$$

where m is the mass of the particle in kg, and v was the particle velocity in m/s.

III. Results and Discussion

HVI tests at RT and ET were conducted using SLG and OLV on individual specimens per test condition as summarized in Table 4. The results of each test are described in the following sections. For each test condition the impacting particle size and impact energy calculated from Eqs. 1 through 4 are presented.

Table 4. FRPC Test Specimens.

Impactor	Test Temperature, °C	Post-Test Comments
SLG	25	Surface divets/craters
SLG	175	Surface divets/craters; delamination, microcracking
OLV	25	Surface divets/craters
OLV	175	Surface divets/craters; delamination, microcracking

A. Soda Lime Glass (SLG)

1. RT Test

In order to establish a baseline, an impact test was performed at RT. Prior to testing, the panel was determined by Ultrasonic inspection to be well consolidated (Fig. 5). After HVI testing, gross visual analysis suggested no detectable damage. The post-impact panel C-scan image was found to exhibit no detectable difference (i.e. damage) compared to the pre-impact panel image (Fig. 5). The white vertical line observed in the post-impact image was due to a support bar in the water tank. Image analysis of the post impact panel under magnification revealed surface damage in the form of divets or craters with depths that were several times the crater diameter.

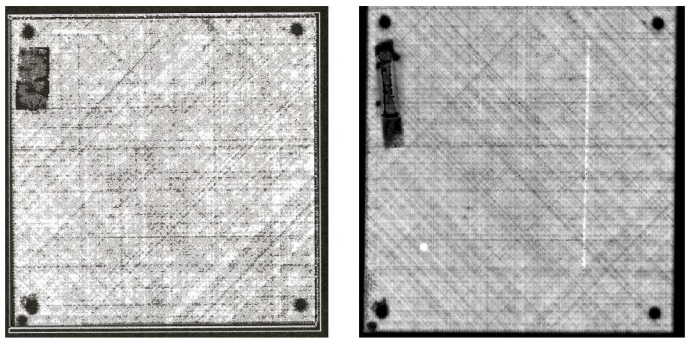

Pre-Impact **Post-Impact**

Figure 5. C-scan of pre- and post-impact RT SLG test panel.

A total of 27 impacts were identified with velocities ranging between 4.8 to 13.2 km/s. Sixteen of the impacts were determined to be from SLG by inspection of the roundness of the corresponding witness film holes. However, 2 of these were too close together to individually assign discernable impact velocities. A graphical distribution of the 14 SLG impacts with known velocities is shown in Fig. 6. Not included in Fig. 6 are the other 11 impacts that were attributed to gun debris fibers (G10 fiberglass) and the 2 SLG particles with unknown velocities.

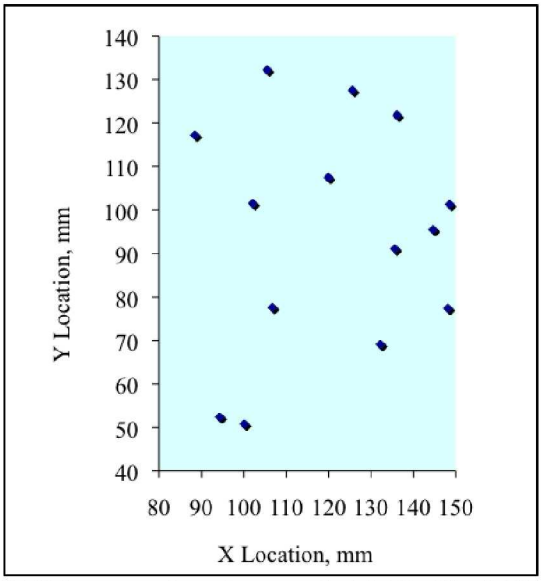

Figure 6. SLG impactor locations on the RT SLG FRPC test panel.

To further assess the effects of the SLG impacts at RT, two specimens were cut and polished from the FPRC. These sections included areas with and without impacts. Photomicrographs of these areas and their respective

location on the FRPC revealed no internal damage (i.e. delamination and microcracking) are shown in Fig. 7. This was further supported by the post-impact C-scan image shown in Fig. 5.

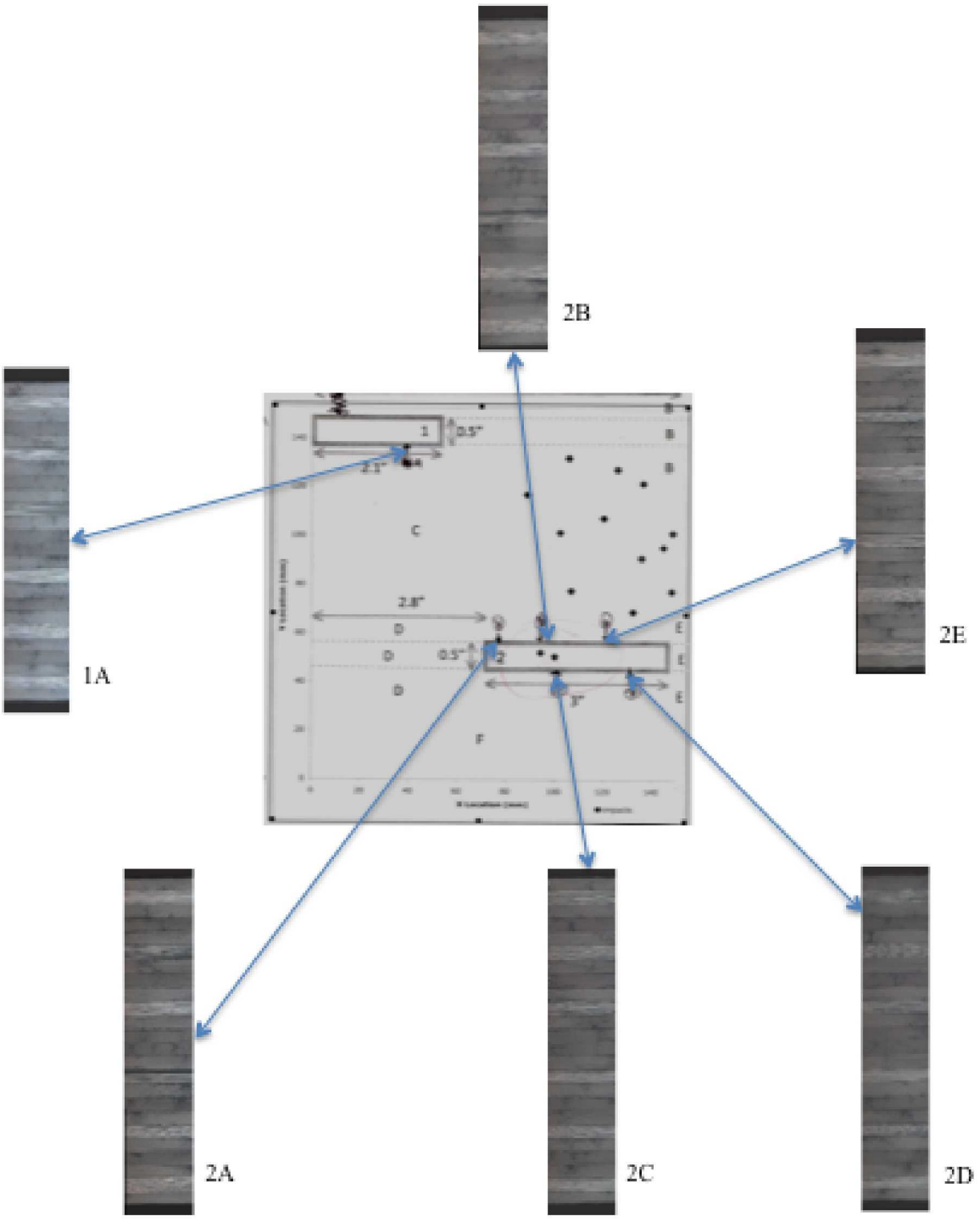

Figure 7. Photomicrograph map of RT SLG FRPC test panel.

The calculated impactor size and energy were determined as previously discussed with the results presented in Table 5. The calculated impactor diameter ranged from 50 to 214 μm with a total calculated energy of ~2 J imparted to the

Table 5. Calculated RT SLG Particle Size and Impact Energy.

Impact Location		Witness Film Dimensions		Impact Area	Velocity, km/s	Calculated Particle diamter, μm	Calculated Energy, J
X	Y	a	b				
mm	mm	μm	μm	μm^2			
100.10	50.80	25.65	24.43	21575	7.6	50.05	0.005
144.60	95.50	51.52	57.66	53944	7.6	108.98	0.047
136.10	121.80	46.78	38.14	67914	7.8	84.46	0.023
88.45	117.20	50.44	85.49	59304	7.8	131.30	0.087
94.31	52.40	82.11	28.28	77113	7.9	96.35	0.035
135.60	91.10	38.62	27.42	43712	8.1	65.07	0.011
106.70	77.60	66.03	23.75	23175	8.6	79.18	0.023
125.60	127.50	79.77	54.77	57835	8.8	132.16	0.112
132.20	69.10	33.52	32.69	22151	9.2	66.19	0.015
148.50	101.30	229.87	26.78	66945	10.6	156.88	0.273
102.10	101.50	56.30	24.44	23083	11.2	74.17	0.032
148.10	77.40	63.46	22.47	26502	11.3	75.50	0.035
105.50	132.20	69.96	31.72	43583	12.3	94.19	0.079
119.90	107.50	59.24	192.62	15451	13.2	213.59	1.067

FRPC during the test (Table 5). The average calculated particle size was 102 μm compared to 68 μm in Table 2. The total calculated particle mass that impacted the panel was 2.99 x 10^{-5} g. No discernable trend was observed for particles of increasing size that were traveling at the same velocity with regards to impact area as shown in Fig. 8A. 2). It was observed though that as the velocity increased the impact area decreased for particles of approximately the

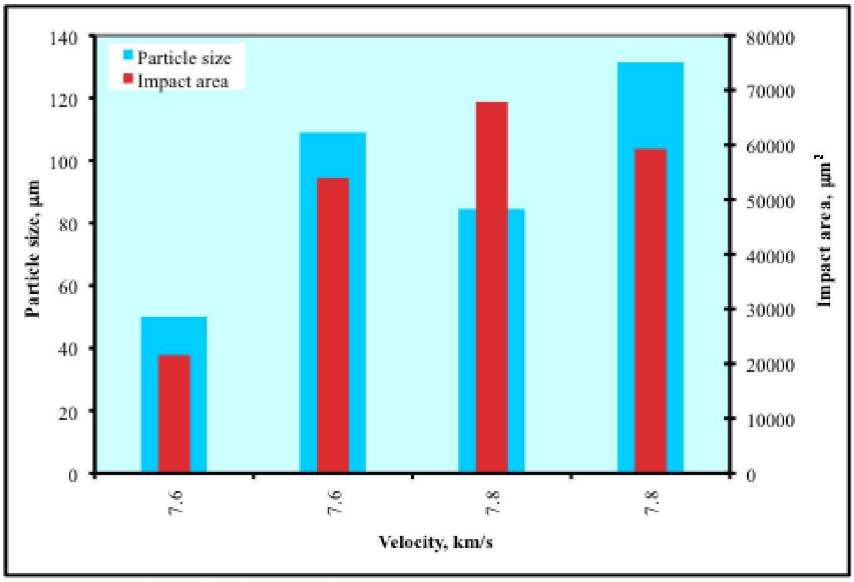

Figure 8A. Particle size and impact area vs. velocity.

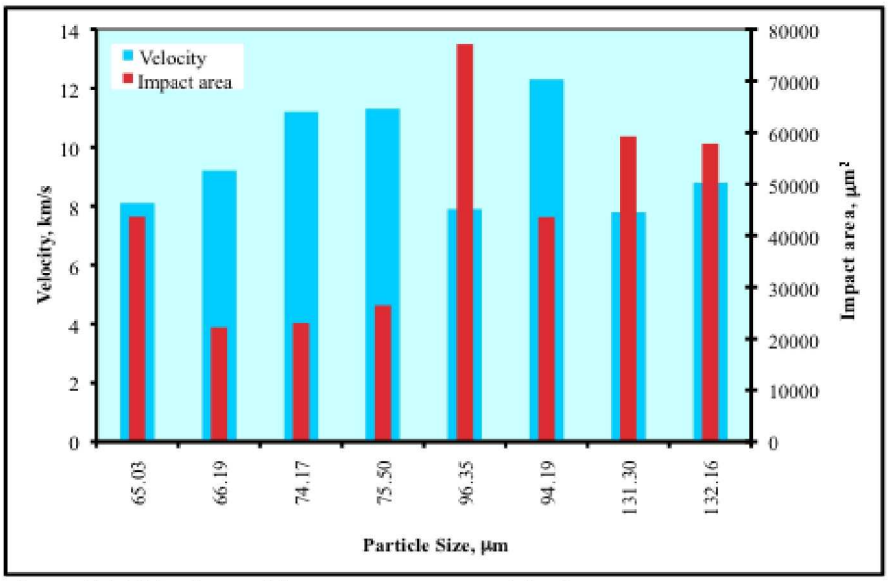

Figure 8B. Velocity and impact area vs. particle size.

same size shown in Fig. 8B. The impact area was comparable for particles that were approximately 75 μm in size traveling at similar velocities.

2. ET Test

Despite the fact that the LEO and Lunar environments include both cryogenic and elevated temperatures, only a few reported studies have been conducted at these temperatures.[16-18] In this study ET HVI testing was performed at 175°C on a pristine panel. The test temperature was chosen based on the upper reported dry service temperature of 177°C for the FRPC.[24] Gross visual inspection of the post-impact panel revealed a depression (i.e. located within circle) in the impact area (Fig. 9) that was larger than expected given the size of the impactor (i.e. average particle diameter of 68 μm in Table 2). This observation was unexpected since heating the FRPC would not have caused such a depression to form. Image analysis of the post-impact panel under magnification revealed divets or craters in the top ply similar to those observed for the RT SLG post-impact panel as well as several parallel cracks in the impact area. These cracks were presumed to be from stress build-up in the FRPC during heating due to the tight fit of the mounting bolts used to secure the FRPC to the test stand.

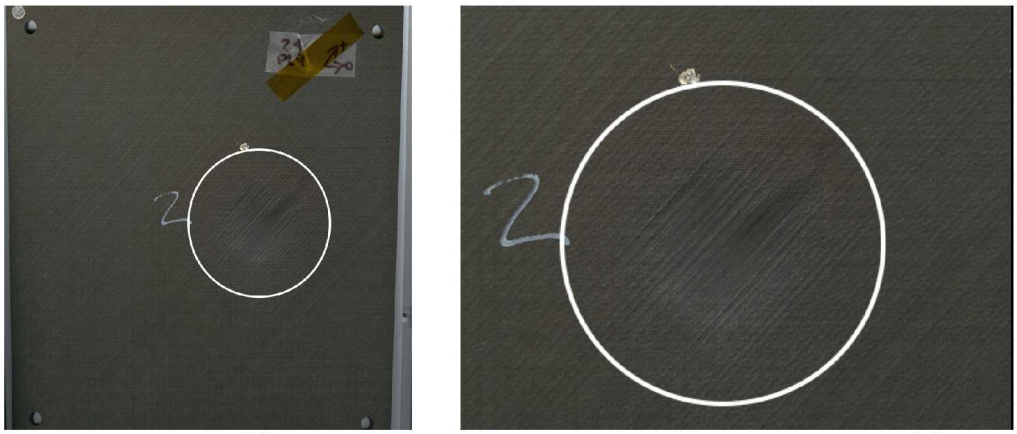

(A) (B)

Figure 9. A) Scanner image of depression on the post-impact elevated temperature SLG test panel and B) Close-up scan of depression.

Based on the visual analysis, the C-scan image of the post-impacted FRPC was of interest. The C-scan image of the post-impacted FRPC in Fig. 10 showed a large circular damage area compared to the pre-impact FRPC. This area was larger than that observed visually on the panel surface (Fig. 9) and was presumably due to delamination.

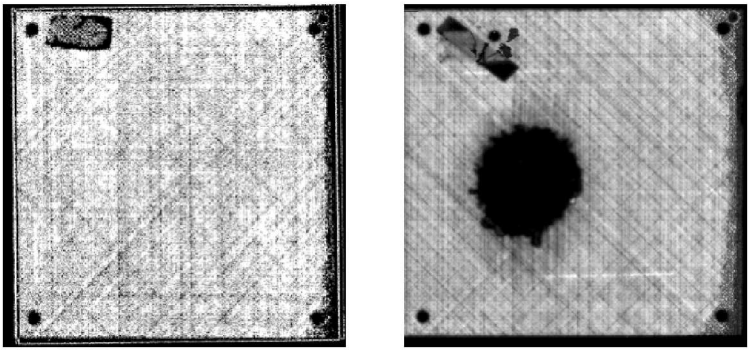

Pre-Impact **Post-Impact**

Figure 10. C-scan of pre- and post- impact ET SLG test panel.

The test resulted in 33 impacts being recorded with velocities ranging from 4.9 to 12.8 km/s and were comparable to those observed for RT testing. For 26 of the impacts, the location, velocity, and impactor crater dimensions were determined. For the other 7 impacts, velocity data was not recorded by the PMT. A graphical representation of the impact locations due to the 26 SLG impactors with known velocities is shown in Fig. 11.

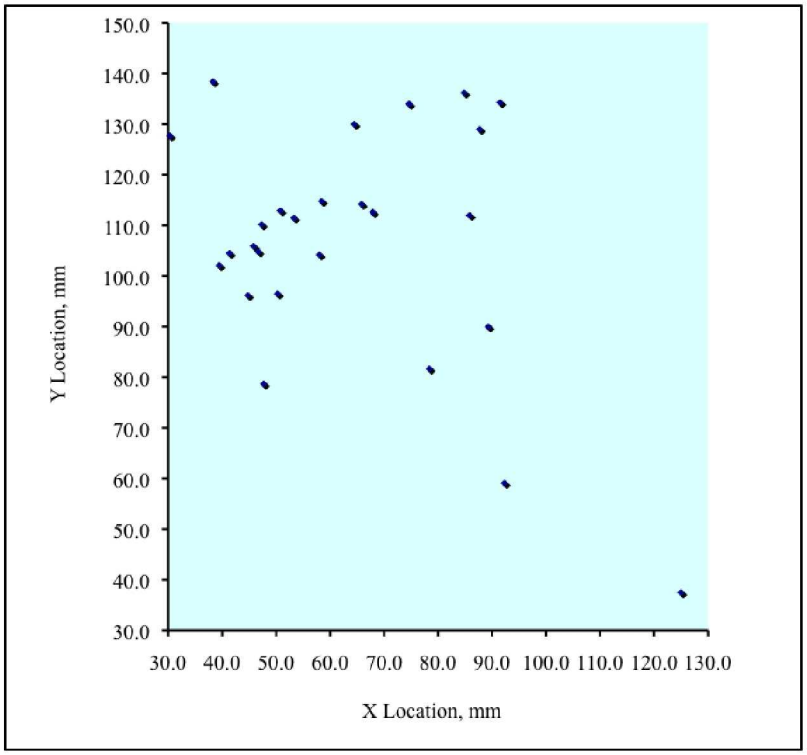

Figure 11. SLG impactor locations on the ET FRPC test specimen.

An overlay of the graphed impact locations in Fig. 11 over the post-impact C-scan image in Fig. 10 was made to view the SLG impacts in relation to the damage area (Fig. 12). The circular image in the overlay in Fig. 12 is a representation of the impact area centered on the bore of the gun barrel. The locations of SLG impactors with known

and unknown velocities identified in blue and red, respectively, are shown in Fig. 12. As seen in Fig. 12, a majority of the SLG impactors resided in the damage area detected by Ultrasonic inspection. A few of the impactors resided outside this area with no perceivable damage other than that observed under magnification. Given the reduction of composite properties at elevated temperature,[15] it was speculated that the resultant damage may have been induced by the generated shock waves from each of the impacting particles through constructive and destructive addition. It has been reported that at elevated temperature the composite toughness of this system was higher, but a lower number of cycles were needed for delamination to occur and faster fatigue crack propagation was observed.[16] This theory may aid in the explanation of the result seen here even though the FRPC was not cycled in this study.

Another possible explanation for the damage observed in the post impact C-scan image is that it was caused solely by heat. The distance between the mounting of the silicon diodes and the heat lamps may have contributed to greater heating in the area in direct line of the illumination than was recorded by the data monitoring system. FRPCs are known to have low thermal conductance. Several diodes were mounted on the FRPC but the sensors were positioned away from the beam to minimize direct heating of the sensors. If the heating method did not achieve a uniform heating, then there may have been an overshoot in sample temperature. However a large damage area is not observed in Fig. 5 outside the impacted area. Therefore this explanation is not complete and requires further work to determine the exact cause of the observed delamination.

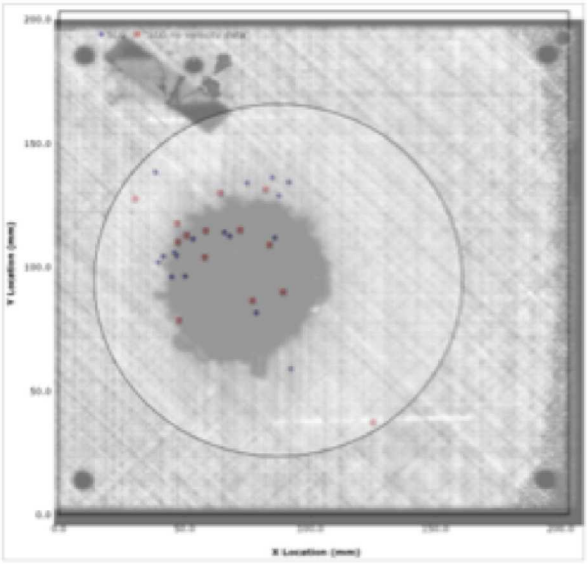

Figure 12. Overlay of post-impact panel C-scan image over graphed SLG Impacts with known (blue) and unknown (red) velocities.

To assess internal effects due to the SLG impactors, two sections were cut and polished from the post-impacted FPRC and photomicrographs obtained. These sections included areas with and without impacts as well as areas within and outside the damage area indicated by the C-scan image. The photomicrographs of these areas and the associated location on the FRPC are shown in Fig. 13. Photomicrographs 1A. 1B, 1J, 2A, and 2B were well consolidated with no evidence of damage. These areas were outside the damage area and devoid of impacts. The remaining photomicrographs revealed numerous microcracks. Photomicrographs 1E and 1F taken in areas within the damage zone also showed delamination as supported by the post-impact C-scan image. Heavy delamination was indicated in photomicrograph 1E.

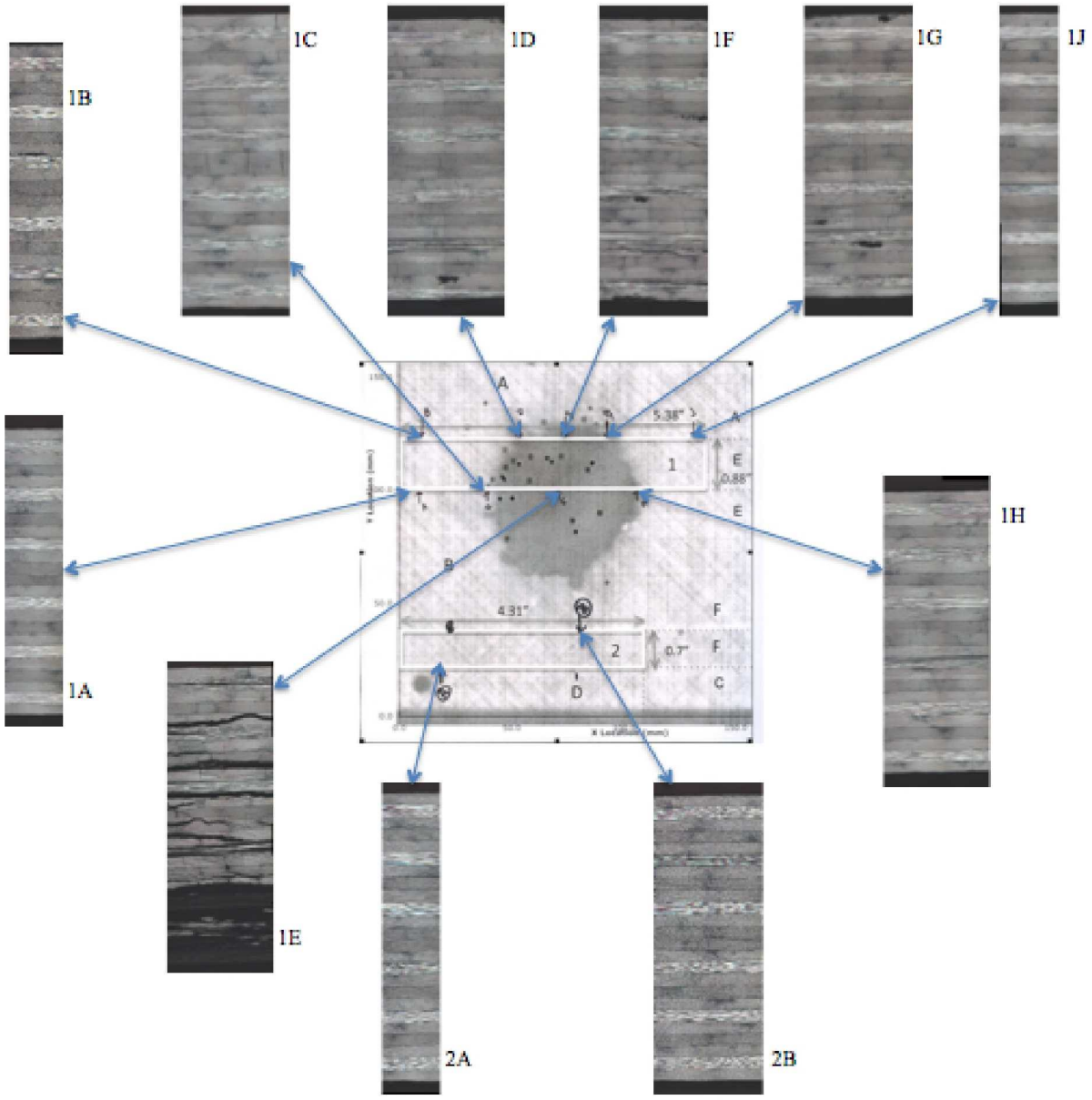

Figure 13. Photomicrograph map of RT SLG FRPC test panel.

Results of microscopic analysis of the impact sites as well as the calculated impactor sizes and energy are tabulated in Table 6. The calculated impactor diameter ranged from 82 to 262 μm with an average size of 136 μm. The total calculated energy and particle mass impacting the panel were approximately 4 J and 1.07 X 10^{-4} g, respectively.

Table 6. Calculated ET SLG Particle Size and Impact Energy.

Impact Location		Witness Film Dimensions		Impact Area	Velocity, km/s	Calculated Particle diamter, μm	Calculated Energy, J
X	Y	a	b				
mm	mm	μm	μm	μm^2			
44.75	96.20	75.05	53.17	82714	4.9	126.31	0.030
38.30	138.40	68.28	54.73	38125	5.6	122.23	0.036
89.30	90.0	99.06	55.16	136943	5.8	147.80	0.068
74.63	134.00	86.83	46.32	65750	6	126.81	0.046
50.80	112.90	61.8	59.48	17630	6.5	121.23	0.047
91.48	134.30	77.76	64.82	92940	6.6	141.96	0.078
58.40	114.80	90.27	75.01	35090	7	164.53	0.137
58.00	104.20	87.34	58.81	3569	7.1	143.30	0.093
30.30	127.70	47.03	46.91	19694	7.2	93.92	0.027
87.68	129.00	71.85	39.38	38528	7.4	106.36	0.041
41.35	104.49	99.45	47.67	34990	7.5	137.67	0.092
47.70	78.70	56.13	34.66	8891	7.6	88.19	0.025
45.81	105.90	268.57	49.17	45234	8.3	229.77	0.525
46.71	104.80	65.57	65.72	64496	8.3	131.26	0.098
47.30	110.20	69.39	40.46	28364	8.9	105.95	0.059
53.30	111.50	104.29	67.28	99981	9	167.49	0.239
64.46	130.00	95.86	61.74	4972	9.4	153.82	0.202
92.30	59.10	83.24	51.39	21600	9.9	130.78	0.138
39.45	102.10	152.14	113.18	165067	10.3	262.38	1.204
67.90	112.60	72.73	61.69	18108	10.7	133.93	0.173
125.00	37.50	66.75	48.7	15053	10.9	114.00	0.111
85.83	112.00	100.44	71.35	21460	11.2	169.27	0.382
65.83	114.20	89.43	57.86	19909	11.9	143.83	0.265
78.38	81.70	77.56	35.81	39958	12	105.38	0.106
50.25	96.50	49.9	33.58	49773	12.1	81.85	0.050
84.83	136.20	44.54	42.49	50724	12.8	86.98	0.068

In general, particles that were approximately the same size in Table 6 exhibited a decrease in the impact area with increasing velocity. This result is shown in Fig. 14 and was similar to the RT SLG observation.

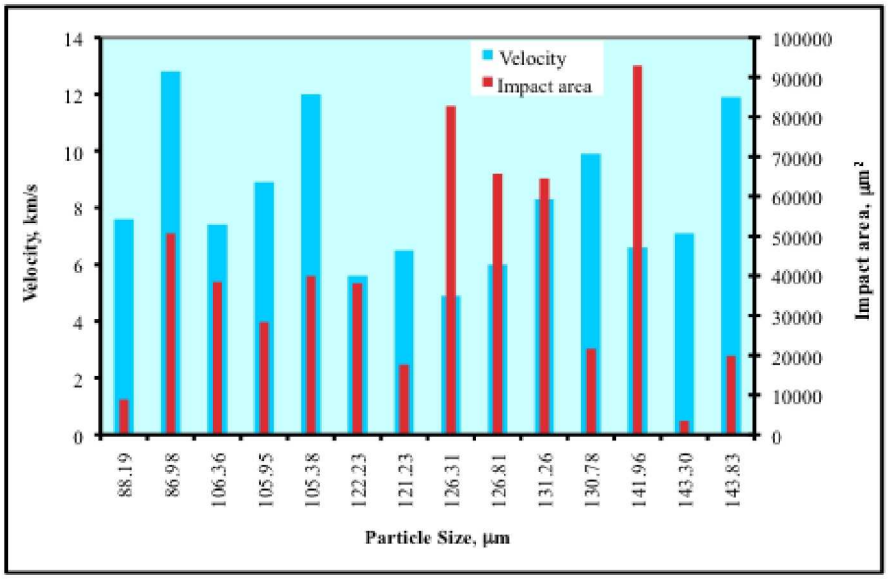

Figure 14. Particle size and impact area vs. velocity.

B. OLiVine (OLV)

1. RT Test

A HVI baseline test was performed at RT using OLV as the impactor. No difference was observed by comparison of the C-scan images of the pre- and post-impact FRPC implying that no internal delamination had occurred (Fig. 15). The white lines in the post-impact image were due to the support bars in the water tank. Post-impact microscopic analysis of the FRPC surface revealed that damage was primarily confined to the top ply in the form of divets/craters with depths that were several times the crater diameter. These results were comparable to those for SLG HVI testing performed at RT.

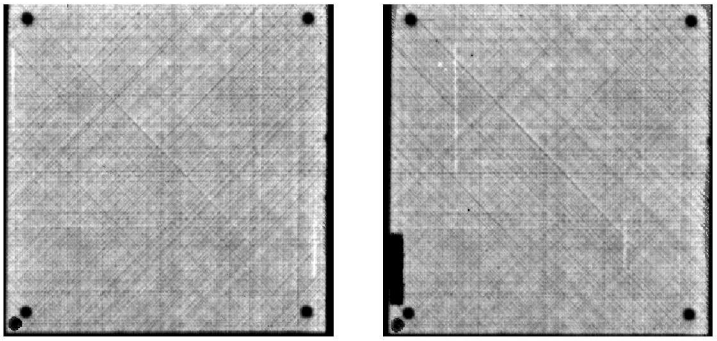

Pre-Impact **Post-Impact**

Figure 15. C-scan of pre- and post-impact RT OLV panel.

For this test, 19 OLV impacts were identified with velocities ranging from 7.7 to 13.3 km/s. For 3 of the impactors, velocity data was not recorded. A graph of the OLV impactor locations with known velocities is shown in Fig. 16.

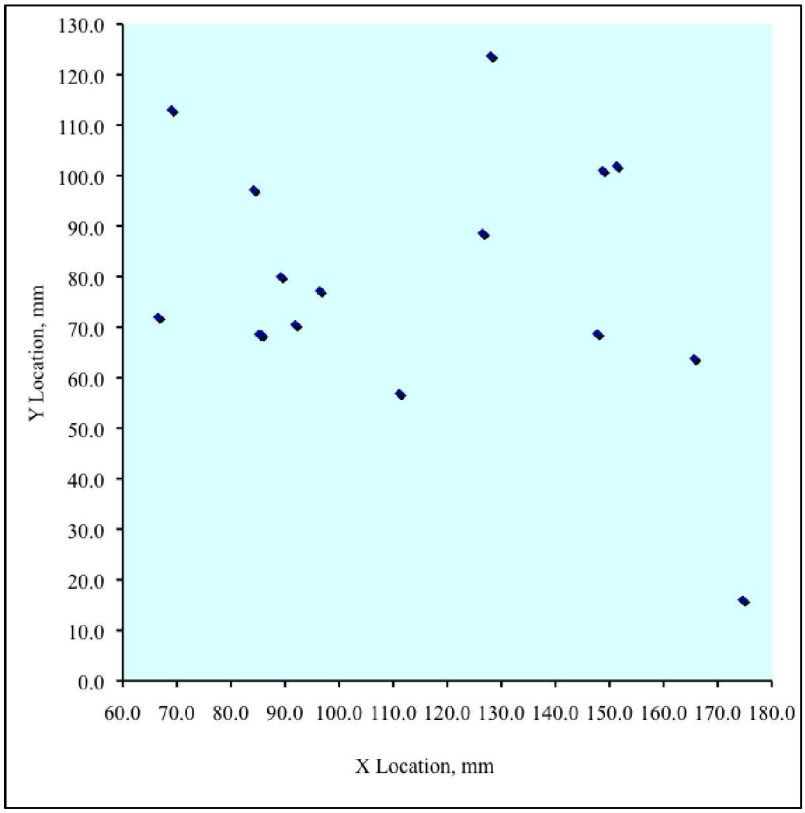

Figure 16. OLV impactor locations on the RT FRPC test specimen.

Two specimens were cut and polished from the OLV RT FPRC test panel to assess the effects of the OLV impacts. The sections included areas with and without impacts and their respective location on the FRPC is shown in Fig. 17. Photomicrographs of these areas revealed no internal damage (i.e. delamination and microcracking) in all areas. This was further supported by the post-impact C-scan image shown in Fig. 15. These results are comparable to the SLG RT test results.

The impact sites as well as the calculated impactor size and energy are shown in Table 7. The calculated impactor diameter ranged from 58 to 266 μm. The average calculated particle size was 128 μm compared to 83 μm in Table 3. The total calculated energy and particle mass that had impacted the FRPC were ~6 J and 9.83 X 10^{-5} g, respectively (Table 7).

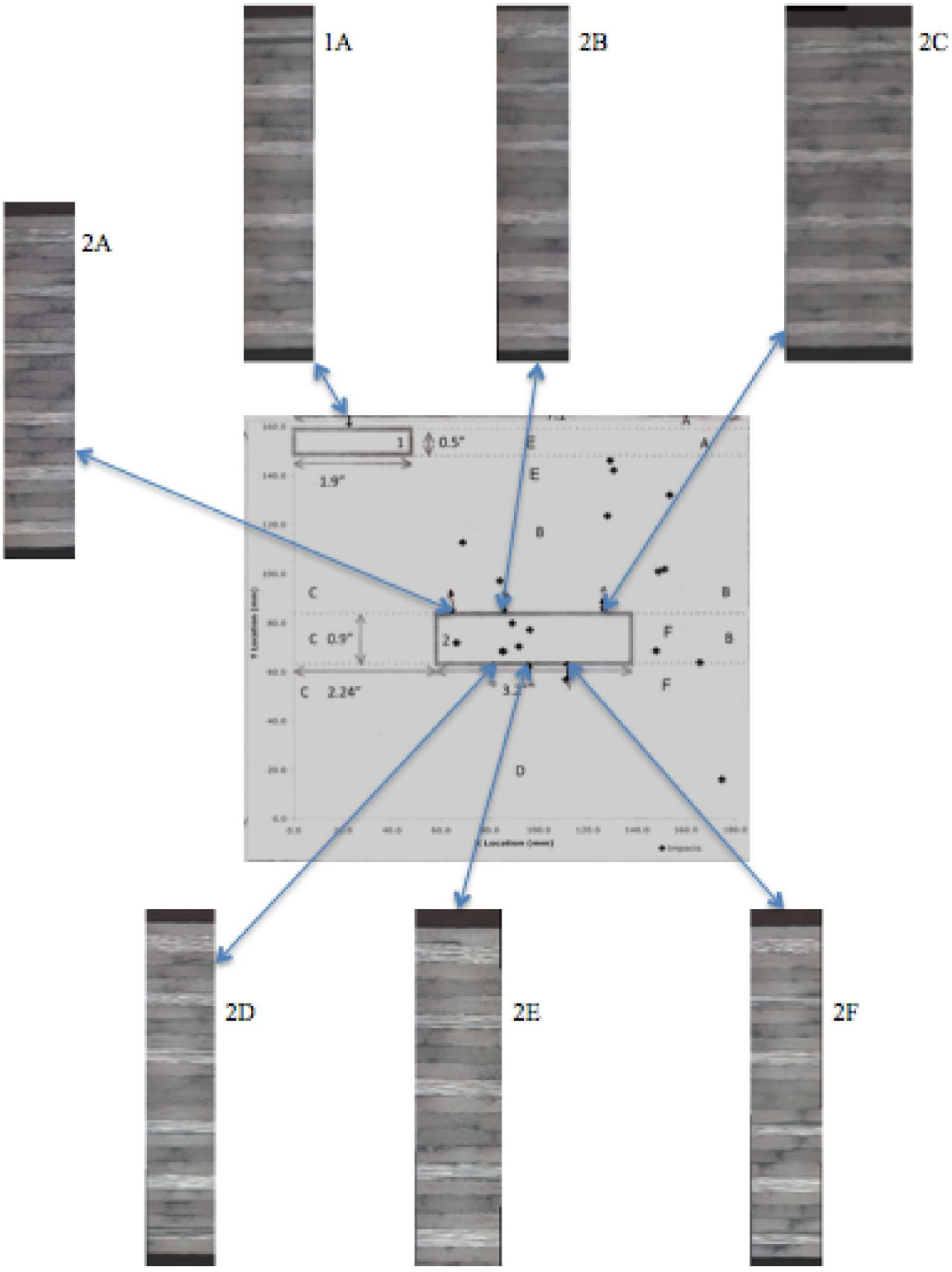

Figure 17. Photomicrograph map of RT OLV FRPC test panel.

Table 7. Calculated RT OLV Particle Size and Impact Energy.

Impact Location		Witness Film Dimensions		Impact Area	Velocity, km/s	Calculated Particle diamter, μm	Calculated Energy, J
X	Y	a	b				
mm	mm	μm	μm	μm^2			
148.7	101.0	144.2	43.7	25736	7.7	158.72	0.199
165.6	63.8	73.9	13.8	74389	9.3	63.85	0.019
85.2	68.6	75.8	21.5	25035	9.4	80.72	0.039
85.6	68.5	265.6	58.5	20504	9.4	249.24	1.146
151.3	101.9	212.3	24.8	54699	9.4	145.08	0.226
111.1	56.9	64.5	12.9	39713	9.5	57.68	0.015
128.0	123.7	72.5	51.5	12768	10.0	122.18	0.153
69.0	113.0	117.4	29.7	38946	10.1	118.07	0.141
84.2	97.2	39.3	38.4	12794	10.9	77.68	0.047
66.5	72.0	58.0	51.9	44388	10.9	109.70	0.131
147.7	68.7	55.4	30.0	15933	11.9	81.51	0.064
126.5	88.6	73.9	36.8	27360	11.9	104.27	0.134
174.6	16.0	63.9	43.4	175372	12.0	105.30	0.141
89.2	80.0	203.0	87.1	32582	12.5	265.87	2.460
91.9	70.5	161.1	56.5	137064	13.3	190.76	1.029
96.4	77.2	133.6	22.5	38690	13.3	109.63	0.195

In general, particles of approximately the same size exhibited decreasing impact area with increasing velocity as shown in Fig. 18A. Similar results were observed for the SLG impactors. For particles that were approximately 105 μm in size with similar velocity, the impact areas differed markedly in contrast to the SLG RT results where the

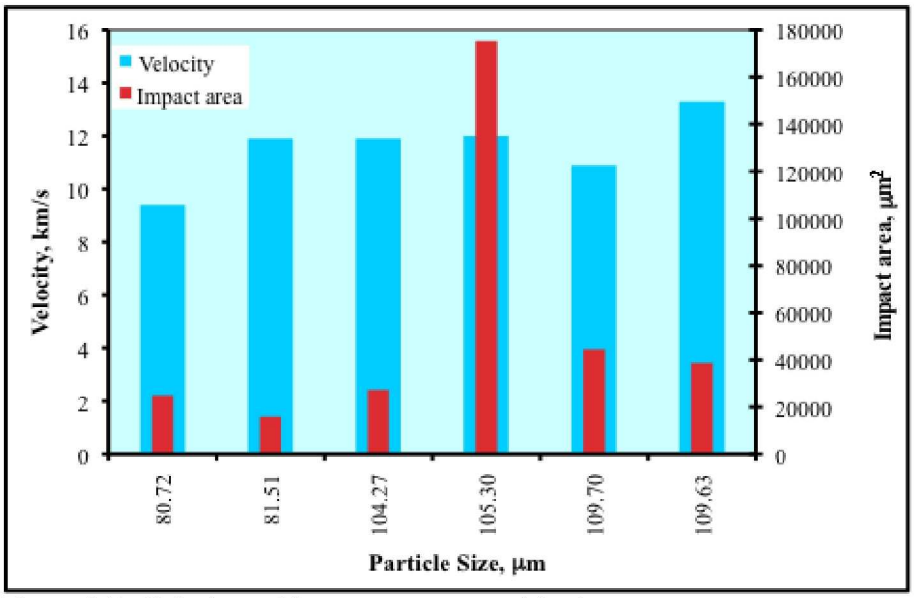

Figure 18A. Velocity and impact area vs. particle size.

impact areas were comparable for similar particle size and velocity. Since the particle size is determined from the witness film, the OLV impactor could have fractured prior to impact resulting in a smaller particle size and thus may account for the different impact areas.

The impact area generally increased with increasing particle size for impactors traveling at the same velocity as shown in Fig. 18B. The lower impact area displayed by the particle size of 249 μm traveling at 9.4 km/s may be due to this particle fracturing prior to impact as cited above.

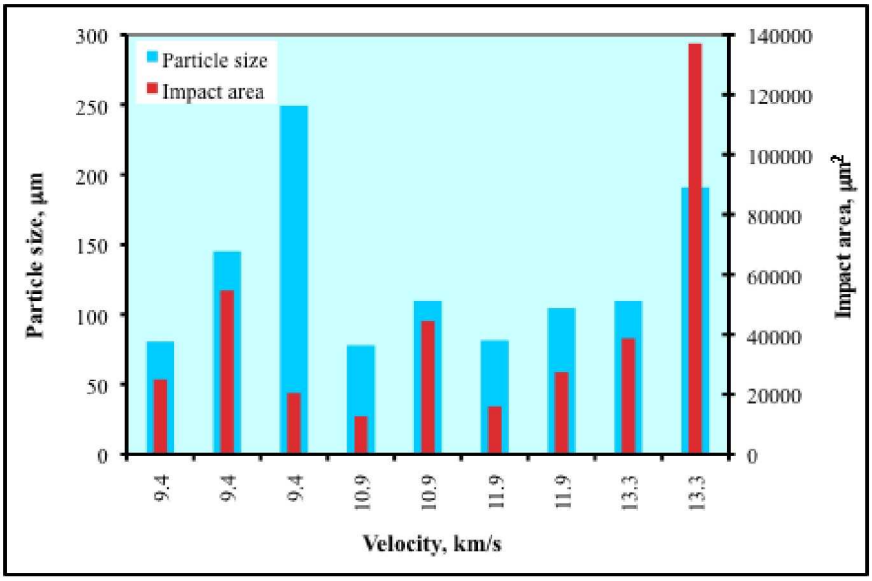

Figure 18B. Particle size and impact area vs. velocity.

2. *ET Test*

Since several parallel cracks were observed in the top ply upon post-impact analysis of the SLG ET test panel and were attributed to stress build-up caused by the size of the mounting bolts used to attach the panel to the test frame, narrower mounting bolts and silicone inserts were used for the OLV ET test panel mounting.

As observed for the post-impact C-scan image of the ET SLG HVI test panel (Fig. 5), the OLV ET post-impact C-scan image showed internal damage (Fig. 19). However, no surface deformations or cracks were apparent upon visual inspection under magnification.

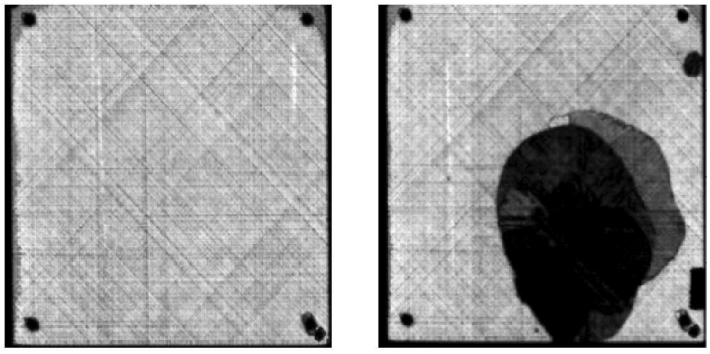

Pre-Impact **Post-Impact**

Figure 19. C-scan of pre- and post-impact ET OLV panel.

Unlike the SLG ET test panel, this panel had been heated twice. The initial test resulted in the gun firing, but no particles were recorded reaching the target based on no flashes being recorded by the PMT and on the streak camera film. Additionally no impacts were found upon summary inspection of the test panel. Therefore it was concluded that the panel was "pristine" resulting in its being used for a retry of the ET test. As a note, the panel had not been ultrasonically inspected after this initial test to see if any internal damage could be observed. The second ET test was successful with the gun firing and data being recorded. The post-impact C-scan image of the panel revealed two different shadings in the impact area (Fig. 19). These two areas may be due to the two different heating events and not from the OLV impactors, or that the first test did provide impacts but with no recorded data. The exact cause is unknown. Further work must be performed to make an adequate determination to the cause of the internal damage observed in the post-HVI C-scan image.

Eleven impacts were recorded with the corresponding locations shown in Fig. 20. The impactors had velocities ranging from 7.5 to 13.9 km/s and were comparable to RT OLV impact velocities.

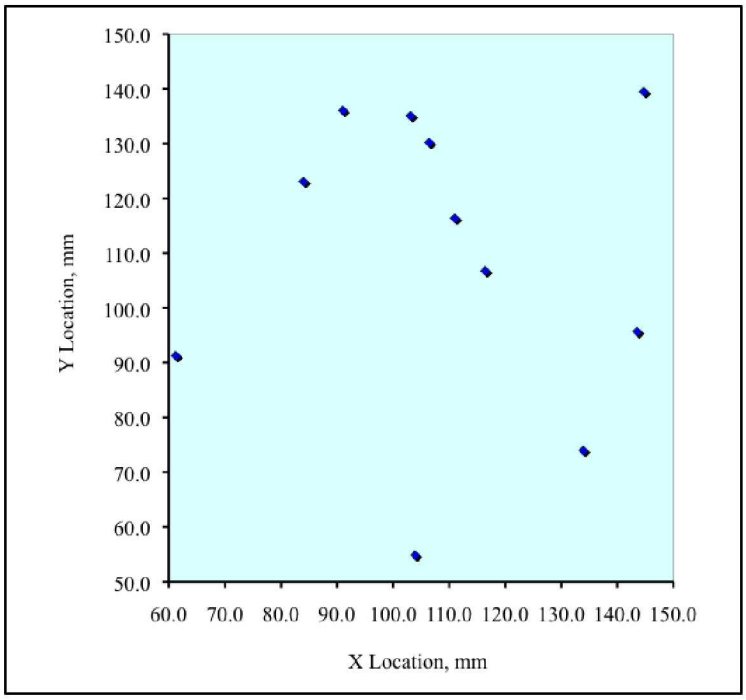

Figure 20. OLV impactor locations on the ET FRPC test specimen.

The relationship between the damage area and the impact locations was evaluated in the same manner as for the SLG ET test panel (Fig. 21). As seen in the overlay, approximately half of the impacts lie within the damage zone. The underlying damage is quite extensive and is greater than that observed for the SLG ET post-test panel. As mentioned this panel had been shot twice, raising the question of whether it was truly "pristine" since it had only been visually examined and not ultrasonically inspected prior to retesting.

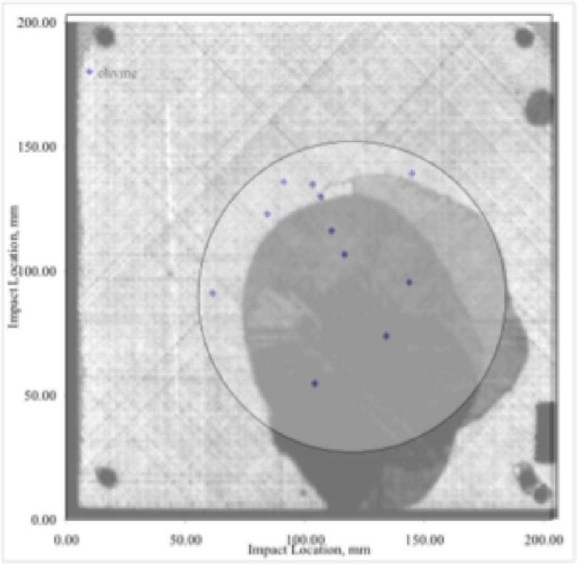

Figure 21. Overlay of post-impact panel C-scan image over graphed OLV impacts.

To assess internal damage, three sections were cut from the post-impacted FPRC and photomicrographed. These sections included areas with and without impacts as well as areas within and outside the damage area indicated in the C-scan image. The photomicrographs of these areas and the associated location on the FRPC are shown in Fig. 22. Photomicrographs from section 2 revealed no evidence of damage as was expected since this area was outside of the damage zone and devoid of impacts. Similar results were observed for the areas shown by photomicrographs 1A and B, 1G, and 3A. Microcracks were observed in the top couple of plies for areas indicated by 1D and 1E. Delamination was observed in photomicrographs 1C and F and 3B and H for the peripheral area of the dark zones as indicated by the C-scan image. The remaining photomicrographs (i.e. 3C-G) were taken in areas within the primary dark area and revealed varying degrees of microcracking and delamination. Even though the OLV and SLG ET test panels were heated differently, the results appear to be comparable.

Results of microscopic analysis of the impact sites as well as the calculated impactor sizes and energy are shown in Table 8. The calculated impactor diameter ranged from 47 to 242 μm with an average size of 124 μm compared to 83 μm shown in Table 3. The total calculated energy and particle mass imparted to the FRPC during the test was ~4 J and 6.71 X 10^{-5} g, respectively.

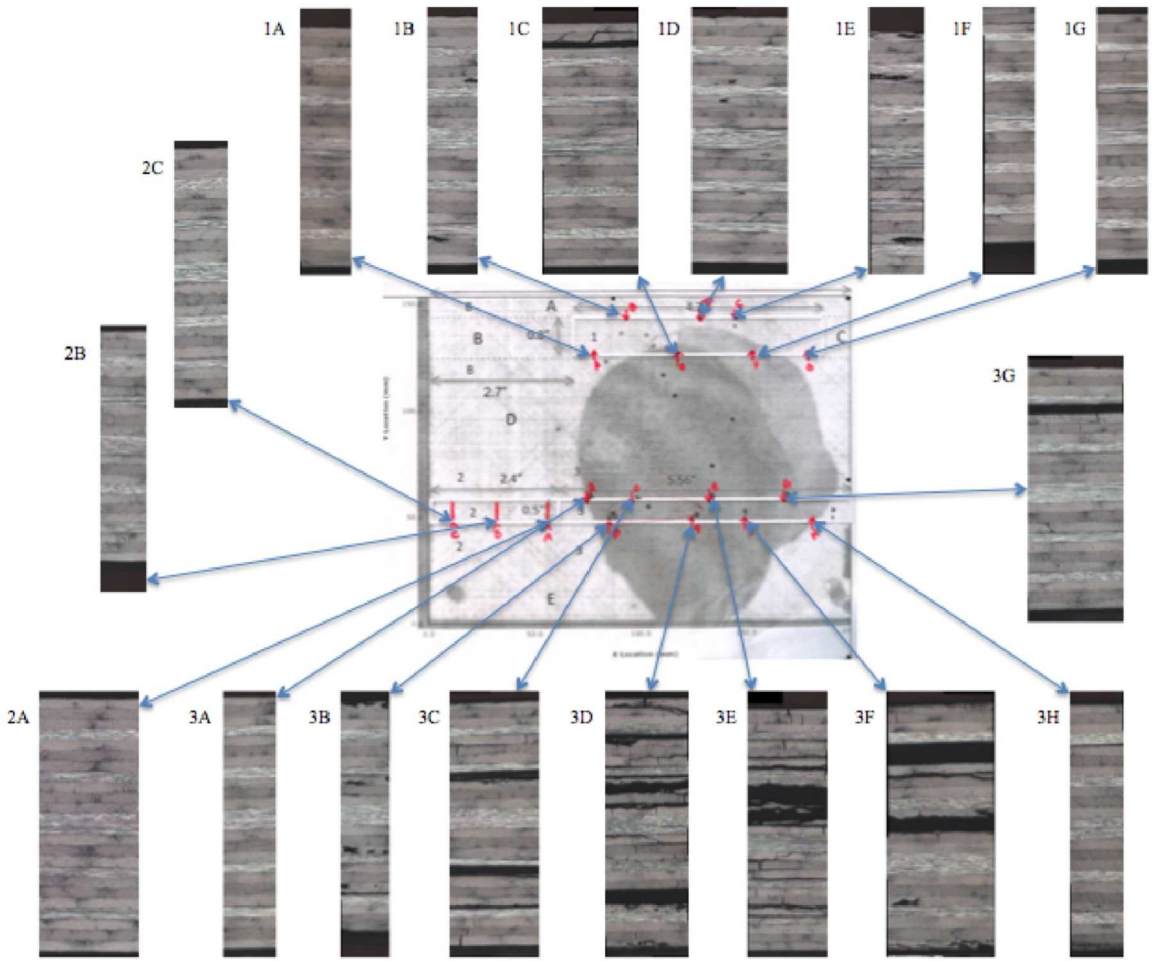

Figure 22. Photomicrograph map of RT OLV FRPC test panel.

Table 8. Calculated ET OLV particle size and impact energy.

Impact Location		Witness Film Dimensions		Impact Area	Velocity, km/s	Calculated Particle diamter, μm	Calculated Energy, J
X	Y	a	b				
mm	mm	μm	μm	μm^2			
61.20	91.30	57.40	49.20	20471	7.5	106.26	0.057
116.40	106.80	126.30	105.90	13345	8.6	231.24	0.766
84.00	123.10	36.50	30.80	14306	10.1	67.04	0.026
91.0	136.10	37.90	20.70	90957	10.8	56.00	0.017
111.00	116.40	227.90	64.50	39535	10.9	242.42	1.418
103.90	54.90	60.1	42	36122	11.5	100.46	0.112
106.40	130.20	61.20	55.50	18107	11.5	116.53	0.175
103.10	135.10	62.10	33.50	65345	12.0	91.20	0.092
133.90	74.00	24.70	22.20	28218	13.2	46.82	0.015
144.70	139.50	185.20	48.80	50493	13.3	190.09	1.018
143.50	95.70	90.60	35.40	21672	13.9	113.24	0.235

For impactors traveling at the same velocity, the impact area did not follow a trend for increasing particle size as shown in Figure 23. One possible explanation for this result is that the particle could have fractured prior to impact resulting in a smaller particle size than the one calculated from witness film dimensions.

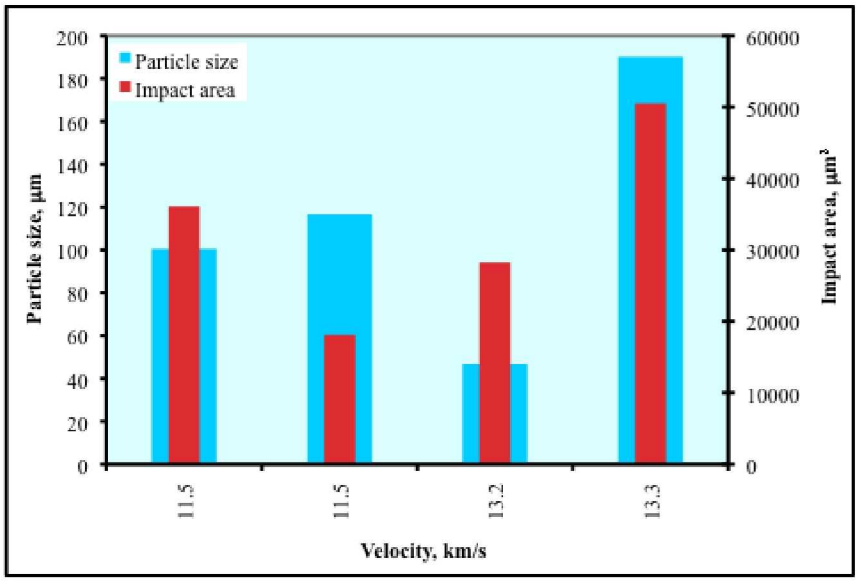

Figure 23. Particle size and impact area vs. velocity.

C. Damage from heat alone?

As described, the heating method for the OLV ET FRPC differed from the SLG ET test in that a heating tape was applied directly to the FRPC backside. Visual assessment of the OLV ET FRPC after placement on a flat surface, prior to sectioning for photomicrographs, revealed a slight but noticeable warpage of the FRPC in the test area. Thus it was of interest to see if the damage effect from the heating event as shown in the C-scan image could be replicated.

A qualitative heating trial was performed on a quasi-isotropic 10.16 cm x 10.16 cm panel to assess what kind of damage may be induced by heat alone. This panel was placed edgewise on a platen with a thermocouple attached to the opposing side of the region to be heated. The temperature was slowly raised until it reached 175°C and was maintained for an hour. During this hold the temperature ranged from 173 to 188°C. Once cooled to RT, warpage of the FRPC surface was observed upon placement on a flat surface. Additionally, there was noticeable discoloration of the area that was in contact with the heated platen surface. Ultrasonic examination of the post-heated panel revealed a delaminated area in this heated region that was not present in the pre-heated C-scan image. To assess the internal damage, a section was cut from this qualitative FRPC and photomicrographs obtained. The photomicrogrpahs and the post-heated C-scan image were overlayed onto the FRPC image as shown in Fig. 24. The delaminated area in the C-scan image can be seen in the lower left-hand corner of the FRPC. Photomicrographs A and E in this area revealed delamination as well as microcracking with image E showing more extensive damage. Comparing image E of this panel with images 3C, 3F, and 3G of the OLV ET FRPC (Fig. 25), one can see that the latter images show that the delaminated area was much more pronounced and separated than in the former. Comparing visual scanned images of the qualitative FRPC and section 3 of the OLV ET FRPC (Fig. 26), the heated qualitative FRPC appears to be pristine in this region while that of the OLV ET FRPC was noticeably delaminated.

One observation from this qualitative heat test was that thermocouple placement on the FRPC had a large effect upon the measured temperature. As previously mentioned, it is known that FRPCs have poor thermal conductivity and thus an overshoot in the temperature could have occurred. Whether the internal damage (i.e. delamination and microcracking) was primarily due to heat alone or in combination with the HVI impactors is still open to discussion.

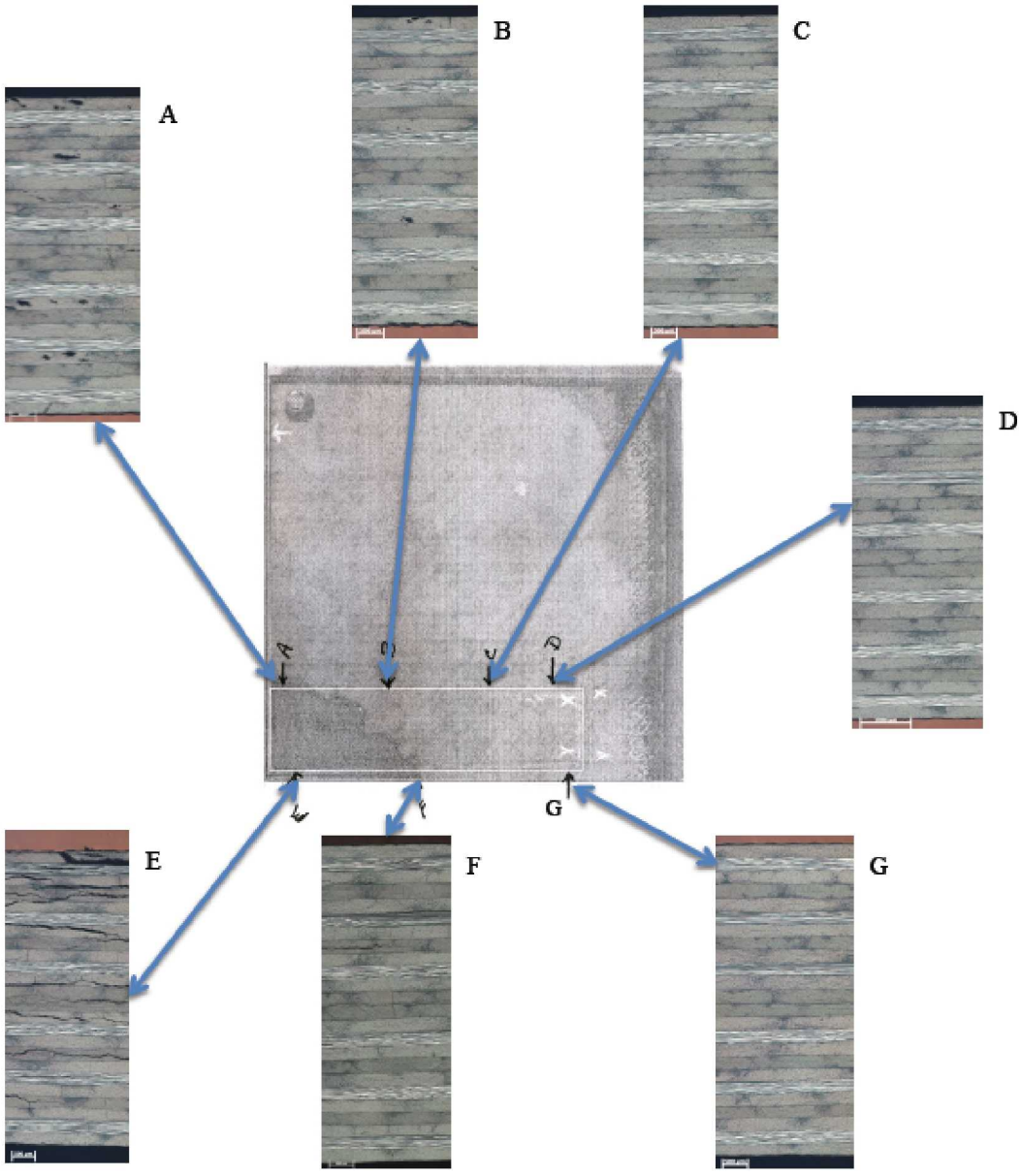

Figure 24. Photomicrograph map of in-house heat treated FRPC.

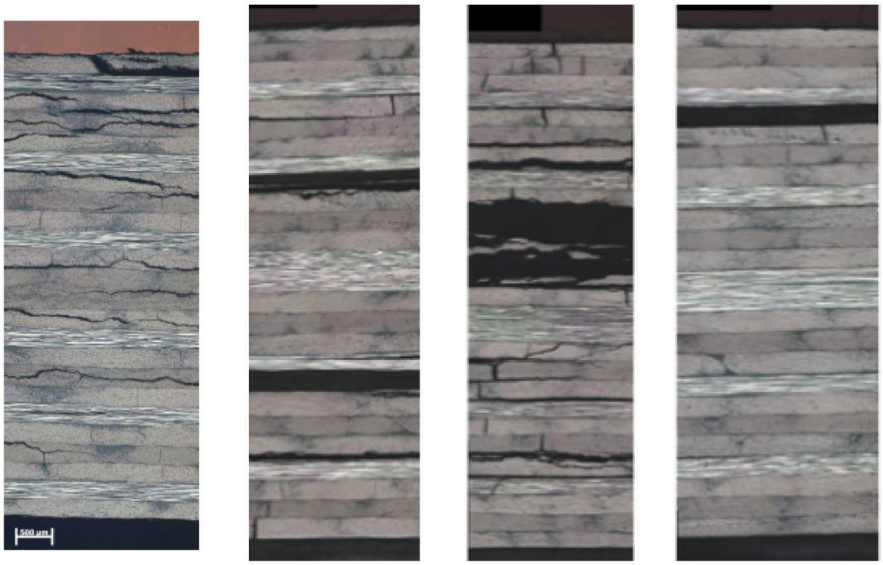

Figure 25. Photomicrographs E and 3C, 3E, and 3G from in-house heat treated FRPC and OLV ET FRPC, respectively.

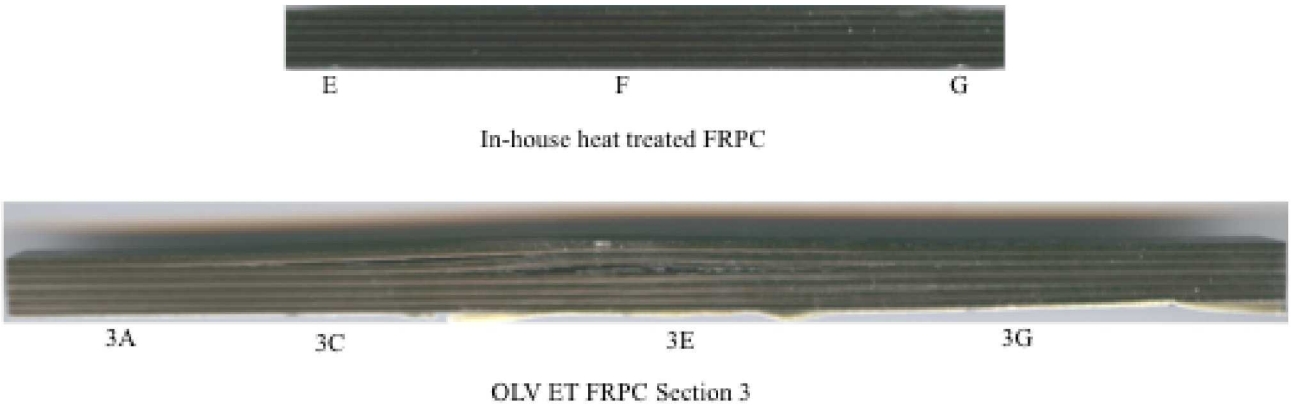

Figure 26. Side view of in-house heat treated FRPC and OLV ET FRPC section 3.

IV. Summary

Flat panels of IM7/977-3 were subjected to hypervelocity (HVI) testing with micron-sized soda lime glass and olivine particles at room temperature (RT) and 175°C. Visual examination under magnification of the post-impacted panels showed divets/craters on the panel surfaces regardless of differences in temperature and particles. C-scan images of post-impacted RT panels were comparable to pre-impact images. Photomicrographs of the RT test panels revealed no internal damage as well. HVI testing at 175°C revealed unexpected internal damage (i.e. delamination) as determined by ultrasonic inspection of post-impacted panels regardless of impactor. A combination of microcracking and delamination was observed in the damage zone for the post-impact elevated temperature test

fiber reinforced polymeric composites (FRPCs). This damage may be due to a combination of reduced material properties at the test temperature and generated shock waves generated from the impacting particles adding constructively and destructively together. A panel exposed to heat alone showed delamination and microcracking, but not to the same extent as the not HVI FRPCs. These results are not definitive as to whether micron-sized particles impacting a hot FRPC are more destructive than impacts on a RT FRPC. It was observed that for the particles with the same velocity as the particle size increased the impact area increased. Additionally particles of approximately the same size showed smaller impact areas as the velocity increased. In conclusion additional HVI work needs to be performed at elevated temperature impacting FRPCs using micron-sized particles to understand the damage behavior.

Acknowledgements

The authors wish to thank Sean M. Britton for the ultrasonic inspection of the panels and James Baughman of Lockheed Martin for the photomicrography of the panels.

References

[1]Tennyson R.C. and Lamontagne, C.G., "Hypervelocity Impact Damage to Composites", Composites: Part A, 31 (2000) 785-794.

[2]Lamontagne, C.G., Manuelpillai, G.N., Taylor, E.A., and Tennyson, R.C., "Normal and Oblique Hypervelocity Impacts on Carbon Fibre/PEEK Composites", Intl. J. Impact Engng, 23 (1999) 519-532.

[3]Lamontagne, C.G., Manuelpillai, G.N., Kerr, J.H., Taylor, E.A., Tennyson, R.C., and Burchell, M.J., "Projectile Density, Impact Angle, and Energy Effects on Hyperelocity Impact Damage to Carbon Fibre/PEEK Composites", Intl. J. Impact Engng, 26 (2001) 381-398.

[4]Lai, S.T., Murad, E., and McNeil, W.J., "Hazards of Hypervelocity Impacts on Spacecraft", J. Spacecraft and Rockets, 39 (2002) 106-114.

[5]Drolshagen, G. "Impact Effects from Small Size Meteoroids and Space Debris", Advances in Space Research, 41 (2008) 1123-1131.

[6]Graham, G.A., Kearsley, A.T., Grady, M.M., Wright, I.P., Griffiths, A.D., and McDonnell, J.A.M., "Hypervelocity Impacts in Low Earth Orbit: Cosmic Dust versus Space Debris", Adv. Space Res, 23 (1999) 95-100.

[7]Cour-Palais, B.G., "Hypervelocity Impact in Metals, Glass, and Composites", Int. J. Impact Engng 5 (1987), 221-237.

[8]Schonberg, W.P., "Protecting Spacecraft Against Orbital Debris Impact Damage Using Composite Materials", Composites: Part A, 31 (2000) 869-878.

[9]Schonberg, W.P. and Walker, E.J., "Use of Composite Materials in Multi-wall Structures to Prevent Perforation by Hypervelocity Particle Impact", Composite Structures, 19 (1991) 15-40.

[10]Katz, S., Grossman, E., Gouzman, I., Murat, M., Wiesel, E., and Wagner, H.D., "Response of Composite Materials to Hypervelocity Impact", Intern. J. Impact Engng, 35 (2008) 1606-1611.

[11]Yew, C.H. and Kendrick, R.B., "A Study of Damage in Composite Panels Produced by Hypervelocity Impact", Int. J. Impact Engng, 5 (1987) 729-738.

[12]Tennyson, R.C., Mabson, G.E., Morison, W.D. and Kleiman, J., "Preliminary Results from the LDEF/UTIAS Composite Materials Experiment", NASA N92-24837, 1992.

[13]Tennyson, R.C. and Manuelpillai, "Analysis of LDEF Micrometeoroid/Debris Data and Damage To Composite Materials, NASA N93-29366, 1993.

[14]Shin, K-B, Kim, G-C, Hong, C-S, and Lee, H-H, "Prediction of failure thermal cycles in graphite/epoxy composite materials under simulated low earth orbit environments", Composites Pt B, 31 (2000) 223-235.

[15]Norwalk, P.S., Sadeh, W.Z., and Janakus, J., "Feasibility Study of Inflatable Structures for a Lunar Base", J. Spacecraft and Rockets, 31 (1994) 453-457.

[16]Myers, B.A., Schonberg, W.P., and Williamsen, J.E., "Temperature Effects on Bumper Hole Diameter for Impact Velocities from 2 to 7 km/s", Intl. J. Impact Engng, 29 (2003) 487-495.

[17]a) Numata, D., Ohtani, K., Anyoji, M., Takayama, K., and Sun, M., "Experimental Study of Hypervelocity Impacts at Low Temperature", Shock Waves, 18 (2008) 169-183; b) Ohtani, K., Numata, D., Kikuchi, T., Sun, M., Takayama, K., and Togami, K., "A Study of Hypervelocity Impact on Cryogenic Materials", Intl. J. Impact Engng, 33 (2006) 555-565; c) Numata, D., Ohtani, K., Anyoji, M., Takayama, K., and Sun, M., "HVI Tests on CFRP Laminates at Low Temperature", Intl. J. Impact Engng, 35 (2008) 1695-1701.

[18]Francesconi, A., Pavarin, D., Giacomuzzo, and Angrilli, F., "Impact Experiments on Low-Temperature Bumpers", Intl. J. Impact Engng, 33 (2006), 264-272.

[19]Vanzani, V., Marzari, F., and Dotto, E., "Micrometeoroid Impacts on the Lunar Surface", Lunar and Planetary Science XXVIII, 1025.pdf.

[20]Ming, D.W. and Henninger, "Use of Lunar Regolith As A Substrate For Plant Growth", Adv. Space Res., 14 (1994) 435-443.

[21]Williams, R.J. and Jadwick, J.J. eds., "Handbook of Lunar Materials", NASA Reference Publication 1057, 1980.

[22]Powell, D., "How Lunar Landers Sandblasted the Moon", http://www.space.com/scienceastronomy/080212-st-lunar-sandblast.html
[23]Cycom® 977-2 Toughened Epoxy Resin Technical Datasheet, Cytec Industries, http://www.cytec.com
[24]Cycom® 977-3 Toughened Epoxy Resin Technical Datasheet, Cytec Industries, http://www.cytec.com
[25]Segal, K.N., "Material Characterization of IM7/977-3 & IM7/5240-4", NASA GSFC Test Report DP09-38, unpublished results.
[26]Wells, B.K., "Cryogenic and elevated temperature hypervelocity impact facility", Intl. J. Impact Engng 33 (2006) 847–854.